Analysis and comparison between rough channel and pipe flows

David Sassun[1], Oscar Flores[2] and Paolo Orlandi[1]

[1] Dipartimento di Ingegneria Meccanica e Aerospaziale - Sapienza Universitá di Roma, Via Eudossiana 16, 00184, Roma, Italia
[2] Dep. Bioingenieria e Ing. Aeroespacial. Universidad Carlos III de Madrid. Avd Universidad 30, Leganes. 28911 Madrid, Spain

E-mail: david.sassun@uniroma1.it

Abstract. Direct numerical simulations of turbulent channel and pipe flows are presented to highlight the effect of roughness at low Reynolds number ($Re_\tau = 180 - 360$). Several surfaces are reproduced with the immersed boundaries method, allowing a one-to-one comparison of the two canonical flows. In general, all rough surfaces produce the same effect on the flow in pipes and channels, with small differences in the roughness function, RMS velocities and spectral energy density of pipes and channels. The only exception is for the rough surfaces made of longitudinal bars. In particular, the triangular bars (riblets) show drag reduction in the channel and drag increase in the pipe. This behaviour is linked to the development of spanwise rollers and wide u-structures near the plane of the crest of the pipe.

1. Introduction

According to the classical theory [1], the inner region of wall-bounded turbulent flows is essentially indistinguishable for the three canonical cases, namely boundary layers, pipes and channels. The differences between these three flows are expected to be limited to the outer region, where mean velocities and standard deviations are expected to scale with the friction velocity and the outer region length scale (boundary layer thickness, pipe radius, or the channel half-height).

However, experimental and numerical studies show differences between these flows in the inner region. For instance, Patel and Head [2] found that the mean velocity in the pipe flow does not follow the logarithmic profile, in contrast to the channel flow. Closer to the wall (i.e., in the viscous sublayer and in the buffer region), the mean velocities of channel and pipe flows collapse, consistent with the notion that sufficiently close to the wall (i.e., at a sufficiently large Reynolds number), the pipe surface appears to be flat. Other studies have confirmed these differences in the log-layer between channels and pipes, concluding that the von Kármán constant κ might not be universal [3] and that the thickness of the logarithmic region might be different for internal and external flows [4].

In terms of the turbulent stresses, the literature also shows differences between the three canonical flows. One of the first studies comparing pipes and channels with Direct Numerical Simulation is Eggels et al. [5], who reported no significant differences of the velocity RMS but a meaningful difference in the skewness of the wall-normal velocity. They claimed that this difference is due to the impingement or splatting process, explained by Mansour et al. [6]. Monty et al. [7], on the other hand, stated that the wall normal and spanwise turbulence intensities differ in the core region of the flows, due to the outer structures that are larger in the pipe than in the channel. Other scholars have found differences in the turbulent kinetic energy between pipes, channels and boundary layers [8], and in the Reynolds stress budget of pipes and channels [9]. Several works [4, 10, 11] connect this differences to the fundamental differences in the large scale motions of the outer region of pipes, channels and boundary layers.

These differences in the outer region of pipes, channels and boundary layers are probably partly responsible for the disparity of results obtained for k-type and d-type roughness in pipes, channels and boundary layers. Based on the data summarized by Jiménez [12], it appears that the turbulent velocity fluctuations between channels and pipes are comparable to each other, while those obtained in turbulent boundary layers seem to scale differently. Borrell [13] argues that it is the entrainment on the turbulent/non-turbulent interface (outer region, large scales) which causes the differences between internal and external flows over rough walls: Kármán's integral equations links the boundary layer growth (i.e., the entrainment) and the friction at the wall (the roughness), resulting in a core region more dominated by entrainment in the case of rough walls. It is important to note that, beside this work, the number of studies analysing the differences between channels, pipes and boundary layers over rough-walls is scarce. To the best of our knowledge, there are no numerical studies comparing one-to-one turbulent flows in channels and pipes with rough walls.

It should be noted that, besides these differences between internal and external flows, there is a wide agreement in the community in that the main effect of roughness in pipes, channels and boundary layers is to shift downwards the mean velocity profile over a smooth wall by a constant amount in the log region, the so-called roughness function. In this paper, we will refer to the roughness function commonly found in literature as ΔU_c^+, and to our definition of it as $\Delta U^+ = \Delta U_c^+ + U_R^+$ where U_R^+ is the slip velocity. The most pressing issue in this regard has been to connect the geometric parameters of the surface to the roughness function. A scaling in this sense has been found recently by Orlandi [14], who derived the relation $\Delta U^+ = B\kappa^{-1}\tilde{v}_R^+$, with B and κ being the log law constants for the smooth wall and $\tilde{v}_R^+$ the RMS of the vertical velocity fluctuations at the plane of the crests. The vertical stress $\tilde{v}_R^+$ is then the fundamental quantity to account for the effects of roughness: if it exceeds a threshold value, the transition to turbulence occurs (Orlandi [15]). A chart of the friction coefficient similar to that by Moody [16], can be calculated by replacing the equivalent sand grain roughness proposed by Nikuradse [17] with $\tilde{v}_R^+$.

The objective of the present work is to establish a one-to-one comparison between channels and pipes for different wall-roughness, in order to understand whether the differences between channels and pipes with smooth walls become more pronounced in presence of the wall corrugation. The paper is structured as follows. In Section 2 and 3, the details of the numerics and of the DNS database are briefly exposed. In Section 4 the results are shown and discussed. These primarily focus on the average velocity and turbulent intensities, the stress and the premultiplied spectra. Finally, in Section 5 the conclusions are presented.

2. Physical and numerical model

The incompressible Navier Stokes equations written in non dimensional cartesian form are:

$$\frac{\partial u_i}{\partial t} + \frac{\partial u_i u_j}{\partial x_j} = -\frac{\partial p}{\partial x_i} + \frac{1}{Re}\frac{\partial^2 u_i}{\partial x_j^2} + \Pi\delta_{1i} \quad ; \quad \frac{\partial u_i}{\partial x_i} = 0 \tag{1}$$

where Π is the pressure gradient required to maintain a constant mass flow rate, u_i is the component of the velocity vector in the i direction, and p is the pressure. The reference values for the non dimensional quantities are either the channel half-height or the pipe radius, both termed h in the hereinafter, and the laminar parabolic Poiseuille velocity at the centreline, u_P. An equivalent set can be written in cylindrical coordinates for the pipe flow, given in Chapter 10 of Orlandi [18]. The equations have been discretized in an orthogonal coordinate system, with a central staggered second-order finite difference method. The integration in time has been made with a third-order low storage Runge-Kutta algorithm, coupled with a second-order Crank-Nicolson scheme. To correct the non divergence-free field, the fractional step procedure is used. Further details are found in [18] and are not repeated here. No-slip boundary conditions are imposed in the non-homogeneous direction. For the cylindrical coordinates a particular treatment at the axis has been used. More details on the numerics for the pipe are found in Verzicco and Orlandi [19]. The periodicity in the homogeneous directions through a Fourier expansion allows to solve the elliptical equation for the pressure directly. The interaction between the flow and the roughness is reproduced by the immersed boundary technique, imposing zero velocity inside the body, and applying a correction to the viscous term at the first grid point near the solid surface. This method is described in detail in Orlandi and Leonardi [20].

3. DNS database

Several simulations of pipes and channels with different wall-roughness are performed at $Re = u_P h/\nu = 4900$. This Re corresponds to a friction Reynolds number $Re_\tau = u_\tau h/\nu \approx 200$ for the smooth channel, where u_τ is defined based on the total stresses at the plane of the crests of the roughness. Note that since the bulk velocity is $u_b = 2/3u_P$ for the channel and $u_b = 1/2u_P$ for the pipe, the bulk Reynolds numbers are different for the two flows: $Re_b = 3266$ for the channel and $Re_b = 2450$ for the pipe. In all the simulations (see Table 1) the size of the computational domain is $L_x = 8h$ in the streamwise direction. The spanwise size of the computational domain of the channel is $L_z = 2\pi h$, in order to make the channel flow comparable to the pipe flow. The coordinates y and z will be used for both the channel and the pipe, where for the latter the wall-normal coordinate is $y = h - r$ and the spanwise coordinate is $z = \theta r$, where r is the radial coordinate.

The database consists of eight surfaces including the smooth case, that will be referred to as SM. The geometry of the rough surfaces is shown in Figure 1 for the channel, where all rough cases have the same roughness height $k/h = 0.2$. For the channel cases, both the upper and lower walls are rough. Note that the roughness is carved into the smooth wall geometry, so that the distance from the plane of the crests to the centre of the channel/pipe is always h. The square and triangular bars placed transversely to the flow (Figures 1a and 1b respectively) will be referred to as ST and TT. For these cases, the cavity width (ST) and the tip spacing (TT) are equal to the height: $s = k$. In these cases, the disposition of the bars makes it necessary to have a large number of nodes in the streamwise direction (801), to accurately reproduce the flow inside

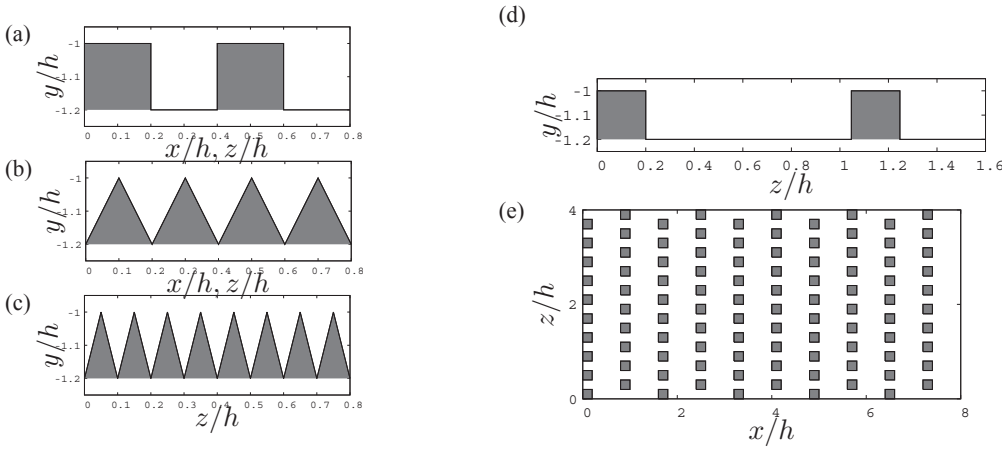

Figure 1: Sketch of the rough surfaces for the channel. (a) square bars longitudinal (SL) or transverse (ST), (b) triangular bars longitudinal (TL) or transverse (TT), (c) longitudinal triangular bars TLS, (d) longitudinal square bars SLL, (e) staggered cubes SC.

		Channel			Pipe		
Case	$n_x \times n_z$	n_y	Re_τ	U_R^+	n_r	Re_τ	U_R^+
SM	801×129	257	204	0	129	169	0
ST	801×129	257	225	0.9	129	218	1.4
TT	801×129	257	290	1.8	129	294	2.2
SL	257×513	257	215	3.2	129	200	3.5
SLL	257×513	257	183	10.8	129	166	12.1
TL	257×513	257	192	6.8	129	178	9.5
TLS	257×513	257	157	6.6	129	162	6.5
SC	801×513	257	347	2	129	361	2.4

Table 1: Computational grid, values of the friction Reynolds numbers and of the slip velocity of the simulations

the grooves. The opposite holds for the longitudinal bars, where the number of points is reduced to 257 in the streamwise direction and increased to 513 in the spanwise/azimuthal direction.

Four cases with longitudinal bars have been simulated: two of square bars, with cavity widths $s = k$ (SL, same as Figure 1a) and $s = 4.236k$ (SLL, Figure 1d, chosen to have six bars in the domain), and two of triangular bars, with tip spacing $s = k$ (TL, same as Figure 1b) and $s = k/2$ (TLS, Figure 1c). A three dimensional geometry made of staggered rows of cubes (SC) is reproduced in Figure 1e. In this case, the number of grid nodes is increased in both directions (801 and 513).

4. Results

Table 1 gives the values of the friction Reynolds numbers for the different runs. Due to the difference in the bulk Reynolds number between the channel and the pipe, the values for SM differ significantly; however, the difference decreases in the rough cases. The transverse bars (ST, TT) and the three-dimensional roughness (SC) increase the value of the Re_τ with respect to the smooth wall, both for the channel and the pipe. However, the behaviour of the longitudinal

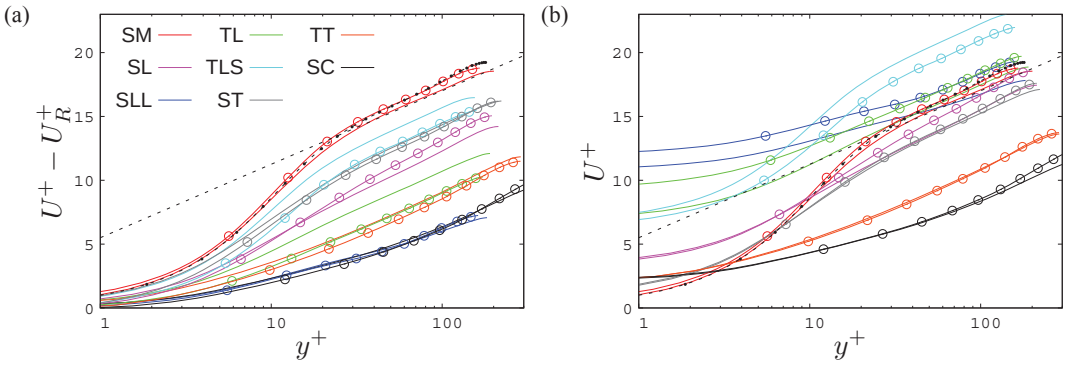

Figure 2: (a) Mean profile in wall units of the velocity minus the slip velocity at the wall U_R^+. The solid lines represent the channel flow, the dotted lines the pipe flow. The solid black symbols are the data by [21]. The roughness function ΔU^+ is evaluated from this plot. (b) Same velocity profile without the subtraction of the slip velocity. The roughness function ΔU_c^+ is evaluated from this plot.

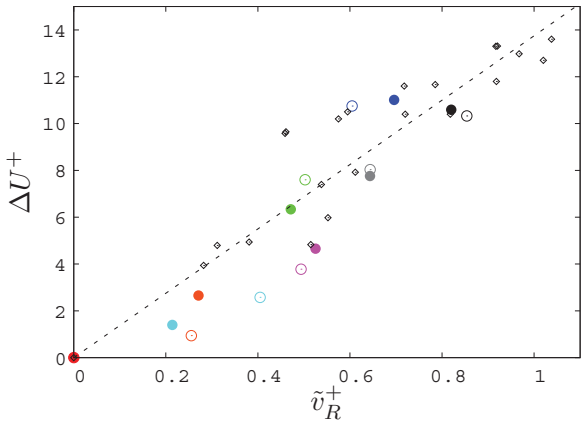

Figure 3: Roughness function ΔU^+ versus the normal stress at the plane of the crests $\tilde{v}_R^+$. Solid circles are the channel, open circles are the pipe, open diamonds are the data by [14], the dashed line is $\Delta U^+ = B\kappa^{-1}\tilde{v}_R^+$, where $B = 5.5$ and $\kappa = 0.4$ are the constants in the log law for the smooth wall.

bars is more variable. The longitudinal square bars (SL and SLL) cause a moderate increase of Re_τ with respect to SM, similar to ST. On the other hand, TL shows an increase of Re_τ in the pipe and a decrease in the channel. For TLS, there is a small decrease in Re_τ in both configurations. We expect therefore that the the riblets will achieve drag reduction. The largest increase in Re_τ is observed for TT and SC, consistently with previous results [14].

The mean velocity profiles of the 16 simulations are presented in Figure 2, where the solid lines correspond to channels and the lines with circles to pipes. The wall normal coordinate is $y^+ = 0$ at the plane of the crests, which corresponds to the position of the wall in SM. The average value of the velocity at this plane is the slip velocity U_R^+ (reported in Table 1), which has been subtracted to the mean velocity profiles plotted in Figure 2a. It can be observed how the velocity profile of SM agrees with the log-law with $B = 5.5$, while the pipe has a slightly higher value of $B = 6$, consistent with Wu and Moin [21]. For transverse square bars ST, a small decrease of the average velocity appears, without an appreciable difference between the channel and the pipe. The transverse triangular bars TT and the staggered cubes

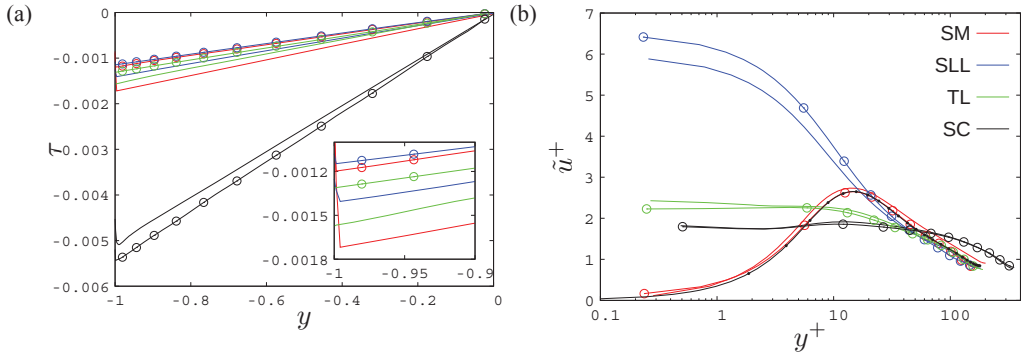

Figure 4: Profile of the the total stress τ (a), and of the normal stress $\tilde{u}^+$ (b), for the lower half of the channel (solid lines) and the pipe (dotted lines). The inset in (a) is an enlargement of the near wall region for the low drag cases.

SC also show the same velocity defect for the channel and the pipe, with the same increase of the roughness function ΔU^+. The largest differences in ΔU^+ between pipe and channel are found among the longitudinal bars cases, TL and SL. The latter also exhibits differences in the slope in the log region. The square bars with wide spacing SLL produce a large velocity defect, but similar for both pipe and channel. It is important to note that the roughness function computed here (ΔU^+) is not the one found commonly in literature: the one evaluated from Figure 2b, that will be referred to as ΔU_c^+ can be rather different. In fact, ΔU_c^+ is the sum of two effects: the slip velocity at the wall U_R^+, representative of the viscous drag, and the roughness function ΔU^+, linked to the form drag. Orlandi [14] gave the relationship between this roughness function and the vertical stress at the plane of the crests $\tilde{v}_R^+$ (the $\sim$ denotes an RMS value): $\Delta U^+ = \Delta U_c^+ + U_R^+ = B\kappa^{-1}\tilde{v}_R^+$, where $B = 5.5$ and $\kappa = 0.4$ are the constants in the expression of the log law for SM. Figure 3 demonstrates that this relationship holds for both channels and pipes.

To understand the difference in the behaviour of the friction, and the drag increase/decrease effect of the roughness on the flow, it is worth looking at the profiles of the total stress $\tau = \nu\partial U/\partial y - \langle uv \rangle$, shown in Figure 4a. In this plot, only the square bars SLL, the triangular bars TL and the staggered cubes SC are reported, since those are the cases with the greater differences between the channel and the pipe. As for the velocity profiles, both SC flows show large differences with respect to SM flows, leading to the conclusion that the wall curvature does not affect the total stress, and in particular the turbulent stress, which is much larger than the viscous stress. The square bars SLL, despite the large ΔU^+ in Figure 2a, show drag reduction for both flows. In this case, the reduction is due to the large decrease of the viscous stress, due to the large U_R^+ at the plane of the crests. The turbulent stress is large, but does not compensate the reduction of $\nu dU/dy$. The large ΔU^+ and the low friction coefficient are not contradictory. In fact, due to the large slip velocity, ΔU_c^+ is small, and the relationship between the roughness function and the friction coefficient (Hama [22]) can be satisfied. The TL flows are the more surprising, showing drag reduction in the channel and drag increase in the pipe.

The profiles of the RMS of the streamwise velocity component are reported in Figure 4b, showing no substantial differences between channel and pipe runs for a given roughness. The

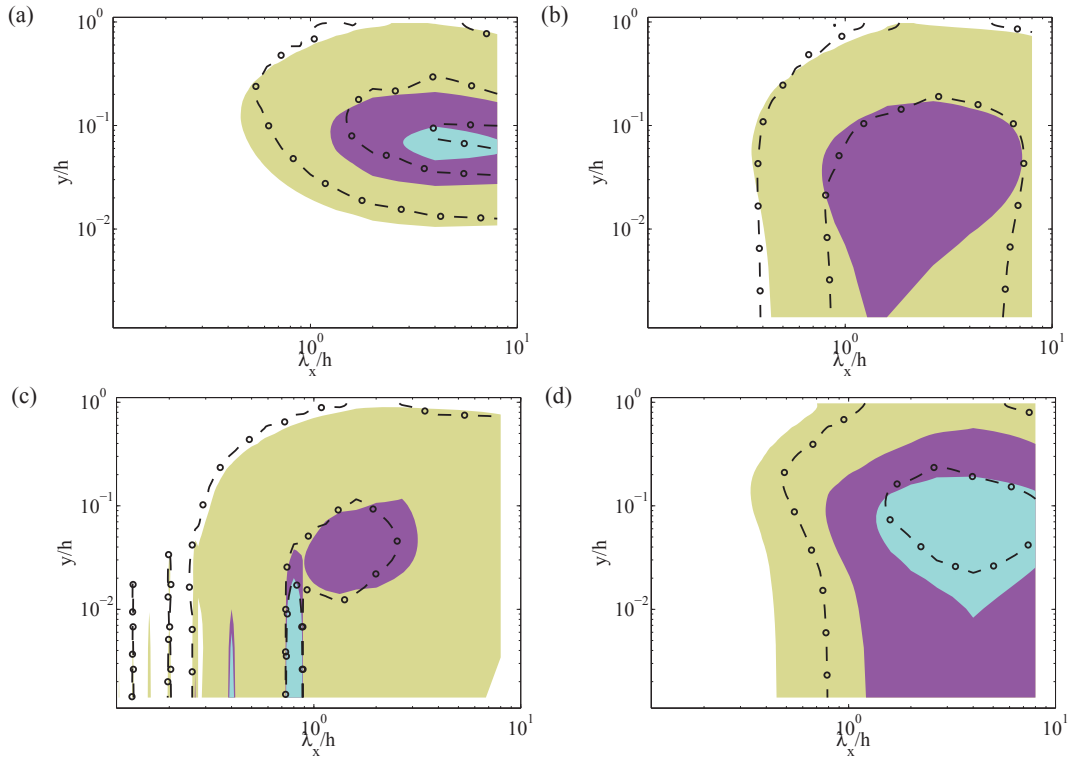

Figure 5: Premultiplied one dimensional spectra of u in the streamwise direction $k_x^+ E_{uu}(\lambda_x^+)$, as a function of the distance from the wall. The filled contour represents the channel and the black contour lines represent the pipe. (a) SM, (b) TL, (c) SC, (d) SLL. The levels are the same in all figures, and are 10%, 50% and 90% of the maximum in SM.

SLL case exhibits the largest $\tilde{u}^+$ at the wall, consistent with a relatively large value of the slip velocity (see U_R^+ in Table 1). This behaviour is consistent with the recent results of Vanderwel and Ganapathisubramani [23], who investigated the effect of the spanwise spacing of longitudinal square bars on boundary layers. They found that a spacing of $s/\delta = 0.88$ results in the largest secondary flow, very similar to the spanwise spacing of case SLL, $s/h = 0.85$. They also reported that the profile of $\tilde{u}$ is maximum in the vicinity of the roughness, which is confirmed by our results. The vertical and spanwise stresses show similar trends as those for $\tilde{u}^+$ and therefore are not presented here.

The RMS profiles suggest that the distribution of velocity fluctuations with y is very similar in pipes and channels with the same roughness. It is however interesting to check if the same can be said about the characteristic wavelengths (sizes) of the structures containing that energy. That information can be obtained from the spectral energy density of the velocity fluctuations, presented in Figures 5-7. Only planes above the plane of the crests of the roughness elements are plotted.

Figure 5 shows the one dimensional premultiplied spectrum of the streamwise velocity fluctuation, $k_x E_{uu}(\lambda_x/h, y/h)$, normalised with u_τ and h. Coloured contours are for the

channel flows, and the chain lines are for the pipe. The differences between the smooth channel and pipe (Figure 5a) near the wall (below $y/h \approx 0.5$) are mostly due to the difference in Re_τ. Both cases show a peak peak located at $y/h \approx 0.07$ ($y^+ \approx 15$), at a wavelength $\lambda_x/h \approx 8$, that corresponds to the position and length of the near wall streaks. However, the differences in the outer region also ($y/h = 0.7 - 1$, $\lambda_x \approx h$) do not seem to be a Re_τ effect, since similar differences have been reported between smooth-walled channels and pipes at higher Reynolds numbers [9, 24].

The spectra for the longitudinal bars (triangular in Figure 5b, square in Figure 5d) show the presence of long energetic structures near the plane of the crests, characterized by a broad peak around $\lambda_x/h \approx 2 - 3$. This peak seems to be shifted towards longer wavelengths for the pipes. It is interesting to note that, for case SLL (Figure 5d) the spectrum of the pipe flow is less intense than the channel's, despite the agreement of the profiles of the RMS of the streamwise velocity perturbation in Figure 4b. This apparent contradiction between the RMS profiles and the spectra is explained by the energy in the $k_x = 0$ modes, which is not represented in Figure 5: for SLL, the pipe flow has more energy in infinitely large structures than the channel flow, an effect that apparently persists through the whole flow thickness. Comparing TL and SLL for pipes and channels, there is no apparent correlation between the streamwise length of the u-structures near the plane of the crests and the drag reduction/increase behaviour of the roughness.

Comparing the longitudinal bars with the staggered cubes (Figure 5c), the latter show short isotropic structures near the plane of the crest. The sharp vertical peaks in the spectrum correspond to the streamwise periodicity of the cubes and its harmonics. The peak about $y/h \approx 0.05$ is damped in case SC compared to SM, consistent with the damping of the buffer region cycle by the roughness [25].

The information of the streamwise/wall-normal spectra is complemented with the spanwise/wall-normal spectra shown in Figure 6. Again, the one dimensional premultiplied spectrum for the streamwise velocity is shown, $k_z E_{uu}(\lambda_z/h, y/h)$. Note that for the pipes, the spanwise wavelength is defined in terms of the arc length in the circumferential direction. Hence, as y tends to h (i.e., as we move from the wall to the center of the pipe), the available spanwise wavelengths shrink. This is clearly observed in SM (Figure 6a), where the channel spectrum is roughly aligned with $\lambda_z \propto y$, while the pipe spectrum turns towards smaller wavelengths near the centre of the pipe. It is possible that this effect is responsible for the shorter streamwise wavelengths for $y/h \gtrsim 0.7$ discussed before (Figure 5a). Near the wall, both the pipe and channel over smooth walls show a peak at $\lambda_z/h \approx 0.5$, which roughly corresponds to the spanwise spacing of the near wall streaks, $\lambda_z^+ \approx 100$.

The spectrum for TL (Figure 6b) shows the direct effect of the surface roughness in a sharp energy peak at $\lambda_z \approx 0.2h$, which corresponds to the spanwise spacing of the bars. This peak extends up to $y/h \approx 0.07$ ($y^+ \approx 12$). Note that the peak for the pipe appears at a slightly smaller wavelength, which is probably a consequence of the curvature of the wall. For the channel, we can observe several harmonics at smaller wavelengths. For the pipe, these harmonics are less intense, and do not show in the spectrum. Moreover, the spectrum for the pipe is wider near the plane of the crest than that of the channel. For the SLL case (Figure 6d), we can also observe a dominant peak at $\lambda_z \approx h$ (close to the spacing of the bars), with stronger harmonics than in TL. However, in contrast to TL, for SLL the u-structures of the channel near the plane of the crest are wider in the channel than in the pipe. In general, the flow structures generated by SLL are stronger than those generated by TL, and have a stronger influence in the outer flow.

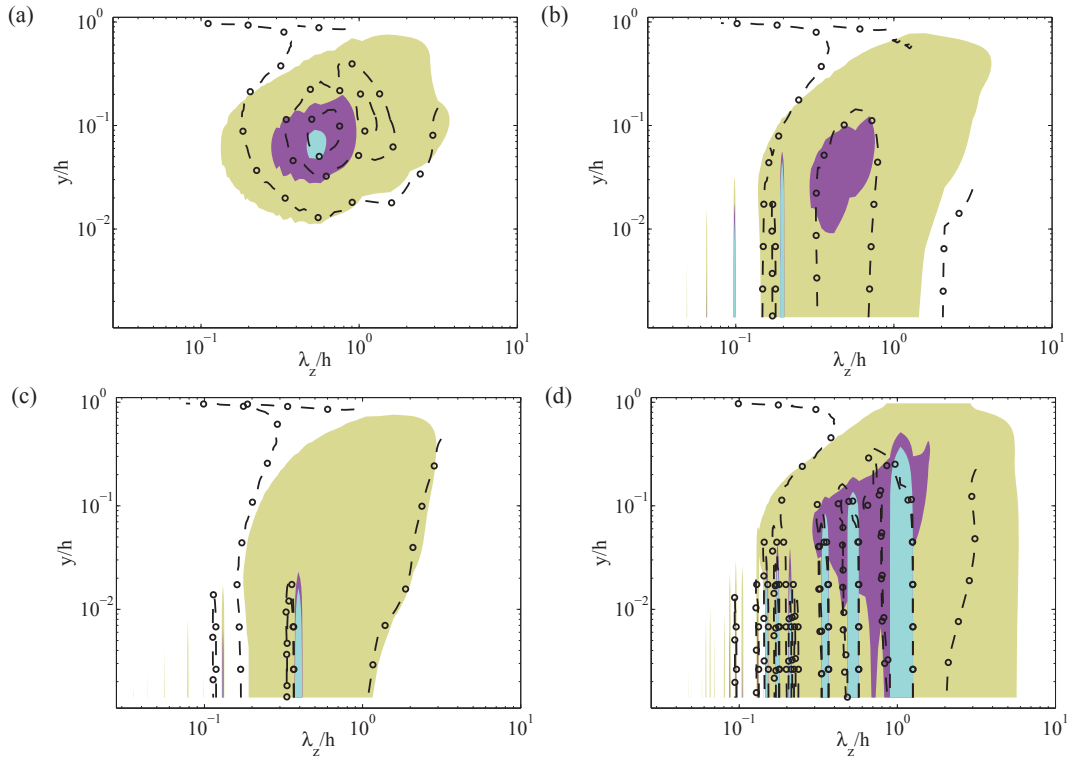

Figure 6: Premultiplied one dimensional spectra of u in the spanwise direction $k_z^+ E_{uu}(\lambda_z^+)$, as a function of the distance from the wall. The filled contour represents the channel and the black contour lines represent the pipe. (a) SM, (b) TL, (c) SC, (d) SLL. The levels are the same in all figures, and are 10%, 50% and 90% of the maximum in SM.

For SC, (Figure 6c), it is possible to observe an intense peak near the plane of the crests at $\lambda_z = 0.4h$ ($\lambda_z^+ \approx 140$), a wavelength equal to that of the spanwise spacing of the staggered cubes. In this case, the peak is localized closer to the plane of the crests than in TL. The effect of SC on the near-wall peak is stronger than TL, consistent with the previous discussion of Figure 5. Although it is not visible in Figure 6c because of the levels chosen for the contour, the near-wall peak is still present around $y^+ \approx 15$ and $\lambda_z^+ \approx 100$, although with a lower energy content than in SM and TL.

Finally, it is interesting to note that the SC case shows a very similar behaviour for pipes and channels near the plane of the crests. However, the spectra of TL and SLL for pipes and channels show differences near the plane of the crests: TL in pipes develops wider u-structures at the plane of the crest than in channels, while the opposite is true for SLL (at all heights). It is interesting to try to link these differences to the drag increase/decrease behaviour of these cases. According to García-Mayoral and Jiménez [26], the break-up of the drag reducing regime of riblets can be tracked to the appearance of spanwise rollers on the crest of the riblets, due to an inflectional instability of the mean velocity profile. This instability is given by the permeability condition of the plane of the crests, which is why these rollers are not present over a smooth

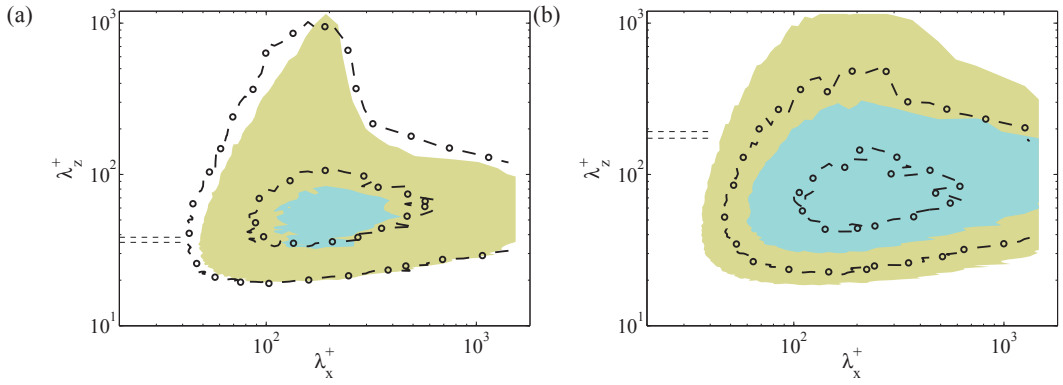

Figure 7: Premultiplied two dimensional spectra of v, as a function of the streamwise and spanwise wavelengths, normalised in wall-units. The levels are 10% and and 50% of the maximum of the spectra of case TL. The spectra are plotted at $y^+ = 5$. (a) Case TL. (b) Case SLL. The horizontal dashed lines mark the wavelength of the roughness. The filled contour represents the channel and the black contour lines represent the pipe.

wall. The analysis of García-Mayoral and Jiménez shows that these rollers are more apparent in the two-dimensional premultiplied spectra of the wall normal velocity, which is plotted for cases TL and SLL in figure 7. The plot shows that for SLL (Figure 7b), the spectra is essentially limited by the spanwise wavelength of the bars (indicated by the horizontal dashed lines in the figure). The most apparent difference between the pipe and the channel is the overall intensity of the spectra, consistent with the differences in the RMS observed in Figure 4b just above the plane of the crests. For case TL, the spectrum is mostly on the sub-harmonics of the spanwise spacing of the bars, and it shows the presence of rollers: very wide structures, with streamwise wavelengths of the order of $\lambda_x^+ \approx 150$, or $\lambda_x \approx 0.8h$. The rollers are more intense in the pipes than in the channel, which might explain why the former are drag increasing while the latter are drag reducing. Stronger rollers might be also responsible for wider u-structures at the plane of the crest for TL in the pipe as compared to the channel.

5. Conclusions

Direct numerical simulations of the flow in turbulent channels and pipes with several surface roughnesses have been performed, allowing a one-to-one comparison between pipes and channels for different wall-roughness at $Re_\tau = 180-360$. The comparison has been established in terms of global indicators of the flow (Re_τ, τ), mean velocity and RMS profiles, and the spectral energy density of the velocity fluctuations.

In terms of global indicators, our results show that the scaling of the roughness function with the vertical velocity fluctuations at the plane of the crest (proposed by Orlandi [14]) works also for pipes. Of the roughness geometries explored here, the largest roughness functions are obtained for staggered cubes and longitudinal square bars with large spacing ($s \approx 5k \approx h$). These roughness geometries produce the largest perturbations in the overlying flow. While for the cubes the perturbations seem not to be coherent at large distances from the plane of the crests, for the longitudinal bars with large spacing the footprint of the roughness is visible in the

spectra up to $y \approx 0.7h$, well into the core region of the flow.

In general, the spectral energy density of the velocity fluctuations of pipes and channels are similar, at least for the wall roughness analysed here. The largest qualitative differences between channels and pipes are found for the longitudinal triangular bars (riblets), which are drag reducing for the channel and drag increasing for the pipe. The streamwise velocity spectrum shows that the u-structures at the plane of the crest are wider in the pipe than in the channel. The analysis of the two-dimensional spectrum for the wall-normal velocity shows the presence of spanwise rollers in both cases, but the rollers in the pipe (drag increasing) are stronger than in the channel (drag reducing), in agreement with García-Mayoral and Jiménez [26].

Acknowledgments

The authors would like to acknowledge the support of the European Research Council, that funded the Multiflow program within which this work was developed.

References

[1] Tennekes H and Lumley J L 1972 *A First Course in Turbulence* (MIT Press)
[2] Patel V C and Head M R 1969 *J. Fluid Mech.* **38** 181–201
[3] Marusic I, McKeon B J, Monkewitz P A, Nagib H M, Smits A J and Sreenivasan K R 2010 *Phys. Fluids* **22** 0651031–24
[4] Jiménez J and Hoyas S 2008 *J. Fluid Mech.* **611** 215–236
[5] Eggels G J M, Unger F, Weiss M H, Westerweel J, Adrian R J, Friedrich R and Nieuwstadt F T M 1994 *J. Fluid Mech.* **268** 175–209
[6] Mansour N N, Kim J and Moin P 1988 *J. Fluid Mech.* **194** 15–44
[7] Monty J P, Hutchins N, Ng H C H, Marusic I and Chong M S 2009 *J. Fluid Mech.* **632** 431–442
[8] Mathis R, Monty J P, Hutchins N, and Marusic I 2009 *Phys. Fluids* **21** 1117031–4
[9] El Khoury G K, Schlatter P, Brethhouwer G and Johansson A V 2014 *J. Phys.: Conf. Ser.* **506** 012010
[10] Monty J P, Stewart J A, Williams R C and Chong M S 2007 *J. Fluid Mech.* **589** 147–156
[11] Lee J, Ahn J and Sung H J 2015 *Phys. Fluids* **27** 025101–16
[12] Jiménez J 2004 *Annu. Rev. Fluid Mech.* **36** 173–196
[13] Borrell G 2015 *Entrainment Effects in Turbulent Boundary Layers* Ph.D. Thesis U. Politécnica de Madrid
[14] Orlandi P 2013 *Phys. Fluids* **25** 110813–12
[15] Orlandi P 2011 *J. Turbul.* **12** N29
[16] Moody L F 1944 *Trans. ASME* **66** 671–684
[17] Nikuradse J 1933 *VDI-Forsch.* **361**
[18] Orlandi P 2000 *Fluid Flow Phenomena - A Numerical Toolkit* (Kluwer Academic Publisher)
[19] Verzicco R and Orlandi P 1996 *J. Comput. Phys.* **123** 402–414
[20] Orlandi P and Leonardi S 2006 *J. Turbul.* **7** N531–22
[21] Wu X and Moin P 2008 *J. Fluid Mech.* **608** 81–112
[22] Hama F R 1954 *Trans. Soc. Naval Archit. Mar. Eng.* **62** 333–358
[23] Vanderwel C and Ganapathisubramani B 2015 *J. Fluid Mech.* **774 R2** 1–12
[24] Ng H, Monty J P, Hutchins N, Chong M S and Marusic I 2011 *Exp. Fluids* **51** 1261–1281
[25] Flores O and Jiménez J 2006 *J. Fluid Mech.* **566** 357–376
[26] García-Mayoral R and Jiménez J 2011 *J. Fluid Mech.* **678** 317–347